Bubble Flow Characteristics in Bubble Columns at Elevated Pressure and Temperature

T.-J. Lin, K. Tsuchiya, and L.-S. Fan
Dept. of Chemical Engineering, The Ohio State University, Columbus, OH 43210

Hydrodynamic characteristics of bubble columns are studied by considering both the local/bubble-scale and global/column-scale properties of the system, with specific emphasis on their dependency on operating pressure and temperature. The local-scale properties include single-bubble characteristics and interactive dynamics involving bubble coalescence and breakup, while the global-scale properties include gas holdup. Experiments are conducted in a bubble column with a multiorifice ring sparger for pressures as high as 20 MPa and temperatures ranging from 27 to 78°C. Density, viscosity, and surface tension, the liquid phase properties, are measured in situ by using hydrostatic weighing, falling-ball and emerging-bubble techniques, respectively. The bubble behavior is examined through direct-flow visualization. Pressure and temperature affect the bubble rise velocity mainly by varying physical properties of the fluids. Effects of pressure and temperature on the rates of bubble formation, coalescence and breakup, and the initial bubble size and maximum stable bubble size are illustrated. Elevating pressure and/or temperature increases gas holdup; the increasing rate depends on the operating conditions through their effects on the fluid physical properties.

Introduction

Bubble-column reactors have gained considerable industrial interest in recent years (Deckwer, 1992). Many reactions that are carried out in commercial processes, such as Fischer–Tropsch synthesis and resid hydrotreating, require operating conditions of high pressure and high temperature (Fan, 1989). Proper understanding of the effects of pressure and temperature on bubble-column hydrodynamics is essential to the optimum design and operation of the reactors. Works available in the literature on both local/bubble-scale and global/reactor-scale properties of bubble columns have been mostly concerned with ambient conditions. The local-scale properties include rise characteristics of individual bubbles and their interactive dynamics involving coalescence and breakup, whereas the global-scale properties include gas holdup. Little is reported regarding the underlying mechanisms of the pressure and temperature effects on these hydrodynamic characteristics.

Studies on the effect of pressure on bubble-column hydrodynamics (e.g., Idogawa et al., 1986, 1987b; de Bruijn et al., 1988; Wilkinson, 1991) have indicated that increasing the operating pressure causes the gas holdup to increase and the average bubble size to decrease. Chiba et al. (1989) and Jiang et al. (1995) reported that the gas holdup increases with increasing pressure up to a point, beyond which there is no significant pressure effect on the gas holdup. By varying operating pressures or by using different gases, Wilkinson (1991) found that the gas holdup increases with gas density, which is consistent with the finding of Idogawa et al. (1986). Through direct flow visualization, Jiang et al. (1995) observed that there is no pressure effect on the Sauter mean bubble diameter for pressures greater than 1.5 MPa.

The interpretation of the pressure effects on bubble-column hydrodynamics in the literature is not fully consistent. Two concepts have been suggested in interpreting these effects. One attributes the pressure effect to an increase in gas momentum (Wilkinson, 1991; Reilly et al., 1994), and the other attributes the pressure effect to a decrease in interfacial tension (Jiang et al., 1992, 1995). The former concept indicates that an increase in system pressure acts in much the same manner as an increase in gas density, while the latter concept indicates that the bubble-size reduction is affected

Correspondence concerning this article should be addressed to L.-S. Fan.
Permanent address of K. Tsuchiya: Dept. of Chemical Science and Technology, The University of Tokushima, Tokushima 770, Japan.

by inherent instability of the bubble surface. Wilkinson (1991) suggested, using an instability analysis, that an increase in gas holdup with an increase in gas density is due to a decrease in the maximum stable wavelength of the gas–liquid interface or the maximum stable bubble size. However, the gas density plays a different role from the pressure, as contended by Clark (1990) in the study of a slurry bubble column and by Kuo (1985) in the study of gas–liquid bubble columns of product wax. They found that the holdup of N_2 is lower than that of H_2, even with a fourteenfold increase in gas density. Clark (1990) suggested that gas holdup is influenced by some pressure-dependent properties other than gas density.

The temperature effect on gas holdup is uncertain due to the lack of consistent data in the literature. Deckwer et al. (1980) found that the gas holdup decreases with increasing temperature in a small slurry bubble column containing N_2, paraffin, and Al_2O_3, while remaining independent of temperature in a large column. Grover et al. (1986) reported the same decreasing trend with temperature for an air–water system. However, they also found that for an air–electrolyte solution, temperature has a positive effect on gas holdup at low gas velocities but has a negative effect at high gas velocities. On the contrary, Zou et al. (1988) and Chabot and de Lasa (1993) both found that elevated temperature always increases the gas holdup in their systems. Zou et al. (1988) attributed the mechanism of temperature effect to a decrease in surface tension and liquid viscosity. In addition, higher temperatures yield higher liquid–vapor pressures, leading to a significant increase in the net gas flow through the column (Wilkinson and Dierendonck, 1990).

Clearly, all of these findings are of direct relevance to the effect of pressure and temperature on the bubble behavior. In a bubble column, bubbles are initially formed at the distributor and rise through the column. The ultimate bubble size in the column depends not only on the initial bubble size but also on the fluid properties as to whether it promotes bubble coalescence or breakup. To quantify the bubble behavior at high pressures and temperatures, it is neccesary to understand the effect of pressure and temperature on the single-bubble rise characteristics such as bubble rise velocity, the bubble dynamics in connection with bubble formation, coalescence and breakup, and the resulting bubble-size distribution.

Two major impediments to the advance in the design of high-pressure and high-temperature bubble columns have been the lack of information on bubble dynamics through direct flow visualization and *in-situ* physical properties such as density, viscosity, and interfacial tension of the gas and liquid. Video-enhanced visualization is essential for the quantification of bubble properties such as bubble size, shape, and rise velocity. Most of the previous studies have addressed the variation of gas density with pressure and temperature, but not of other physical properties of the fluids in the system. Slowinski et al. (1957) and Massoudi and King (1974) found that the surface tension decreases almost linearly with increasing pressure due to gas absorption on the liquid surface. In general, the surface tension also decreases approximately linearly with increasing temperature (Jasper, 1972); for some organic mixtures, however, Deam and Maddox (1970) found that under high-pressure conditions, the surface tension increases with an increase in temperature. The viscosity of most organic liquids can dramatically increase when the system pressure increases (Stephan and Lucas, 1979). It is thus important to know *in-situ* physical properties of the fluids under high pressure and high temperature to characterize the flow behavior of bubble columns operated under such conditions.

In this study, the physical properties of liquid are measured under elevated pressure and temperature conditions. These properties are then used to interpret flow characteristics in bubble columns operated under the corresponding pressure and temperature conditions. The flow characteristics studied include single-bubble rise velocity and gas holdup. Pressure and temperature effects on the rates of bubble formation, coalescence, and breakup are also examined.

Experimental

The following describes the experimental apparatus together with the techniques employed for measurement of liquid physical properties, single-bubble rise velocity, and gas holdup under elevated pressure and temperature.

Flow visualization apparatus

Figure 1 shows the video-enhanced visualization experimental system for high-pressure and high-temperature studies. The system consists of a vertical column, a liquid supply tank, a liquid exhaust reservoir, a piston pump, and a pulsation damper. The vertical column comprises three sections: the plenum, the test, and the disengagement sections. The pipes and column are insulated. Two sizes of stainless-steel columns are used: one is 50.8 mm in diameter and 0.80 m in height, and the other is 101.6 mm in diameter and 1.58 m in height. The latter is specifically used for the bubble rise velocity measurement. In both columns, there are three pairs of planar quartz windows with dimensions of 12.7 mm in width and 92 mm in height. These windows allow viewing through the entire test section of the column. The plane shape circumvents optical distortion in photography.

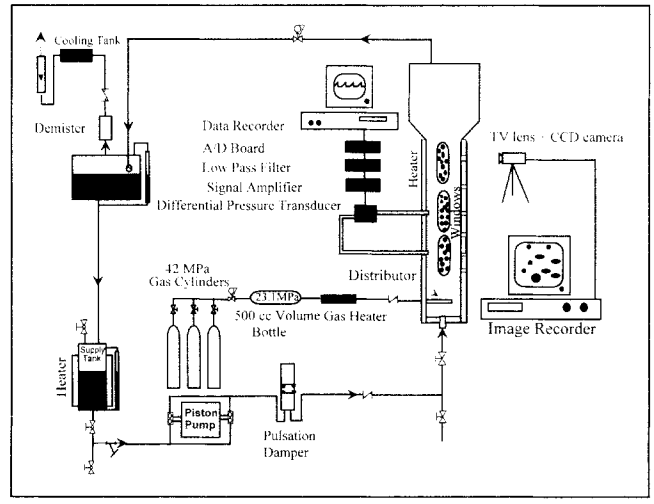

Figure 1. High-pressure and high-temperature bubble-flow visualization apparatus.

Nitrogen, which is supplied from three gas cylinders (42 MPa), is used as the gas phase and as the pressurizing source. The inlet pressure is regulated by a two-stage regulator and the flow rate is controlled by a flow control valve. To maintain a constant system temperature, nitrogen is preheated by a gas heater to the desired temperature before being introduced into the column. Nitrogen enters the bubble column through a multiorifice sparger in a ring arrangement with an orifice diameter of 3 mm. After exiting the bubble column, the gas passes through a back-pressure regulator, which is used to control the pressure of the column. It is then ventilated into atmosphere through the demister and the cooling tank. The gas flow rate is measured with either an electromagnetic gas flowmeter or a rotameter at the end of the gas exhaust line. Paratherm NF heat transfer fluid, a stable organic liquid ($T_b = 327$°C at 0.1 MPa), is used as the liquid phase. In this study, the liquid is operated in a batch mode. The liquid level in the column is maintained near the top of the column so that foaming will not affect the global-scale measurements.

In-situ liquid property measurements

The physical properties of the liquid at elevated pressures and temperatures are measured *in situ* using the 50.8-mm column. The contribution of liquid vapor can be neglected due to its low vapor pressure ($P_v = 20$ Pa at 150°C and 0.1 MPa).

Density and Viscosity Measurements. The density of the liquid at elevated pressures and temperature is determined using the hydrostatic weighing method. The falling-ball technique is adopted to measure the liquid viscosity at elevated pressures and temperatures. Detailed procedures have been described by Lin and Fan (1997).

Surface Tension Measurement. The emerging-bubble technique is applied to measure the surface tension between nitrogen and Paratherm NF heat transfer fluid at various pressures (up to 21 MPa) and temperatures (up to 360 K). A 3.2-mm-OD steel tube is inserted vertically into the column and submerged in the liquid. A stable bubble generated on the tip of the tube is video-recorded by a high-resolution (800× 490 pixels) CCD camera with an infinity lens. The measurement involves two steps. In the first step, the boundary of gas–liquuid interface in Cartesian coordinates fixed on the bubble (see Figure 2) is determined through the image processing developed by Haam (1996). In the second step, the boundary coordinates are then used as the basis to calculate the surface tension (see the Results and Discussion section for specific approaches). The image processing incorporates six substeps (see Figure 3). They include: inverting the gray level of the bubble image; inverting the gray level of background image; subtracting one inverted image from the other; inverting the subtracted image; pasting the reflecting area; and defining the boundary based on the difference of the gray level. The preliminary coordinates of the bubble boundary, which are measured in the pixel coordinates, are converted to the actual physical coordinates with the aid of a microruler attached to the tip of the tube. During the image processing, the physical coordinates of the bubble are obtained using the ruler in every image of the bubble.

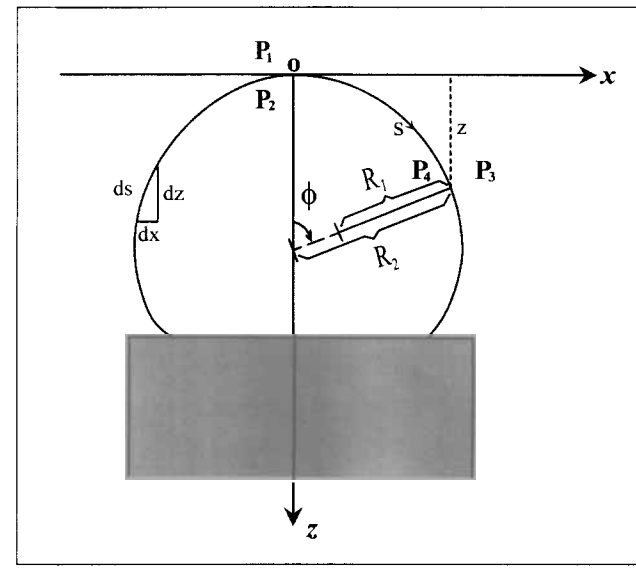

Figure 2. Coordinate definitions for an emerging bubble.

Single-bubble rise velocity measurement

A single-bubble generator is placed at the 101.6-mm column central axis near the bottom window. This bubble generator consists of a Plexiglas cup measuring 17.9 mm in diameter and 21 mm in depth, with its opening facing downward. The cup is fixed on a stainless-steel tubing (3.2-mm OD), through which the gas is introduced into the cup. The amount of gas flowing in is controlled by a pressure regulator and a metering valve. The cup is upended remotely to release a single bubble. A camera (with shutter speed = 1/20,000 s) located in front of the top window is used to record the rise of the bubble. The bubble rise velocity is calculated based on the elapsed time for the bubble to travel over a prescribed distance; the bubble size is also measured through direct visualization.

Gas holdup measurement

The mean gas holdup in the 50.8-mm column is determined using a differential pressure transducer. The transducer is installed 0.50 m ($Z/D \approx 10$) above the gas distributor, which ensures that the measurement of the pressure fluctuations takes place in the developed region. The gas holdup can be related to the dynamic pressure gradient obtained from the differential pressure transducer as

$$\frac{dP}{dZ} = \epsilon_g(\rho_l - \rho_g)g \tag{1}$$

Results and Discussion

In situ liquid properties

Density and Viscosity. Figure 4a shows that as the pressure increases from 0.1 to 21 MPa, the density increases by approximately 5% below the normal boiling point, while the density decreases by approximately 6% as the temperature increases from 293 K to 393 K over the entire pressure range studied. Figure 4b shows that for 293 K, the viscosity in-

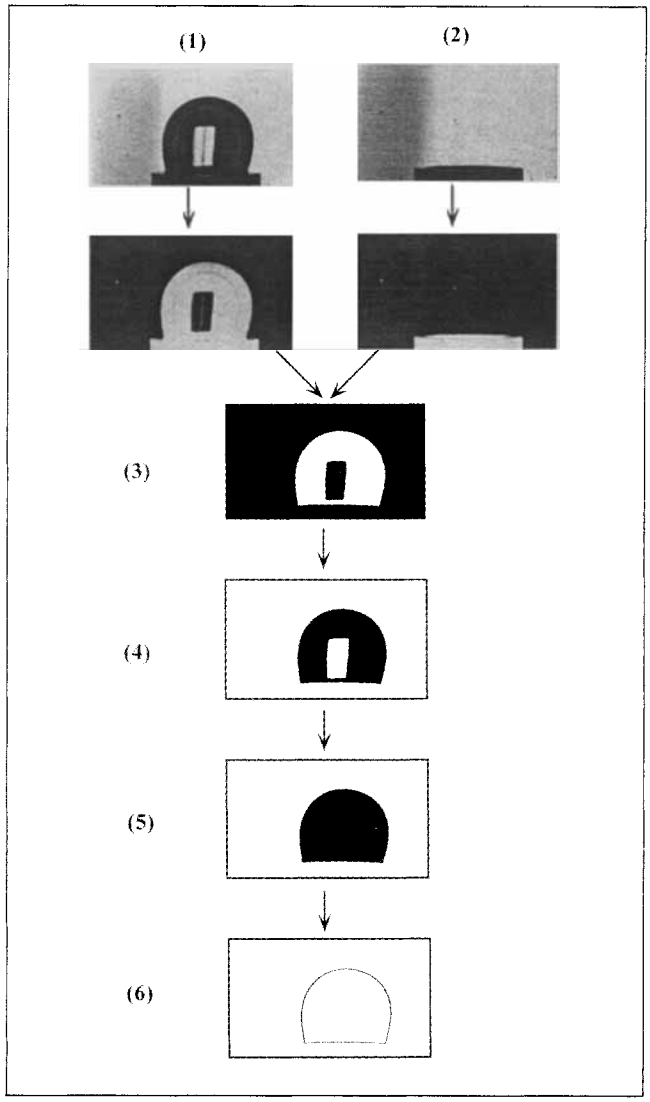

Figure 3. Procedure for background subtraction in image processing of bubble boundary.

creases by 65% as the pressure increases from 0.1 to 20 MPa. For 373 K, however, the viscosity only increases by 10% for the same pressure increase. It also shows that the effect of temperature on the viscosity is more significant than that of pressure over the prescribed ranges; for instance, the viscosity increases eightfold as the temperature decreases from 351 to 300 K at 0.1 MPa.

Surface Tension. There are several methods to measure the surface tension of liquid interfaced with gas bubbles. They include the capillary rise, the du Noüy ring, the Wilhelmy plate, the drop weight, and the pendant/sessile drop (or pendant bubble emerge) methods. In using any of these methods except the last one, it is necessary either to known the contact angle or to assume no friction (for the du Noüy ring and Wilhelmy plate) and equal-drop volume (for the drop weight). The emerging-bubble method is most accurate, and is thus selected for use in the evaluation of surface tension in this study.

When an axisymmetric bubble emerges in the liquid and the bubble is in an equilibrium state (see Figure 2), the pres-

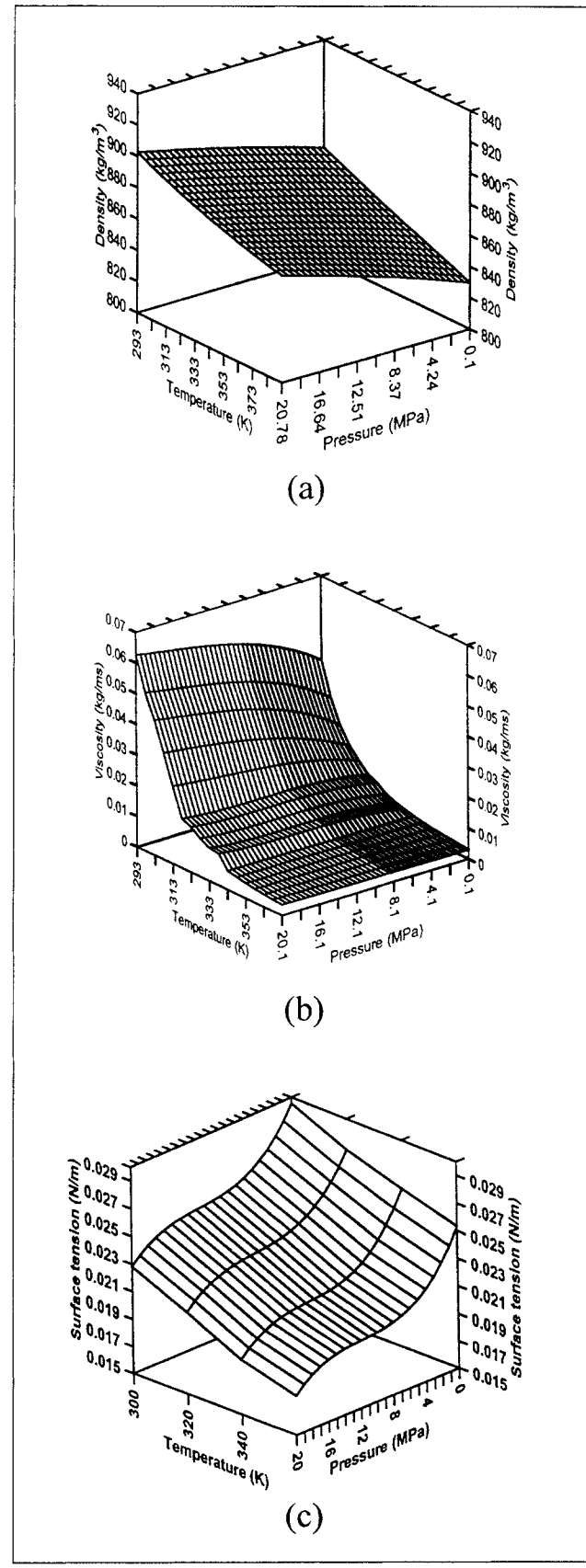

Figure 4. Variations of (a) density, (b) viscosity, and (c) surface tension of Paratherm NF heat-transfer fluid with pressure and temperature.

sure difference across the curved interface can be described by the Laplace equation:

$$\sigma\left(\frac{1}{R_1}+\frac{1}{R_2}\right)=\Delta P, \tag{2}$$

where R_1 and R_2 are the two principal radii of curvature and ΔP is the pressure difference across the interface. At the apex of the bubble, the radius of curvature is R_o ($=R_1=R_2$) and

$$\Delta P_o = P_2 - P_1 = \frac{2\sigma}{R_o}. \tag{3}$$

Discounting all external forces besides gravity, the pressure at any point can be related to that at point P_1 or P_2 by

$$\left.\begin{aligned} P_3 &= P_1 + \rho_l gz \\ P_4 &= P_2 + \rho_g gz \end{aligned}\right\}. \tag{4}$$

Combining Eq. 3 with Eq. 4 yields the pressure difference across any point on the interface

$$\Delta P = P_4 - P_3 = P_2 - P_1 + (\rho_g - \rho_l)gz = \Delta P_o - \Delta\rho gz \tag{5a}$$

or

$$\sigma\left(\frac{1}{R_1}+\frac{1}{R_2}\right)=\frac{2\sigma}{R_o}-\Delta\rho gz. \tag{5b}$$

From trigonometric relationships, it can be shown that $1/R_1 = d\phi/ds$ and $1/R_2 = \sin\phi/x$, where ϕ is the turning angle. Substituting these two relationships into Eq. 5b yields

$$\frac{d\phi}{ds}=\frac{2}{R_o}-\frac{\Delta\rho g}{\sigma}z-\frac{\sin\phi}{x}. \tag{6}$$

Taking the derivative of the trigonometric functions with respect to s yields

$$\frac{dx}{ds}=-\cos\phi \tag{7}$$

$$\frac{dz}{ds}=\sin\phi \tag{8}$$

with the conditions $x(0)=z(0)=\phi(0)=0$.

To calculate the surface tension, Eqs. 6–8 must be solved for several hundred coordinate points on the bubble boundary. Jennings and Pallas (1988) used the rotational discrimination method to obtain an optimized solution for the surface tension, which is adopted in this study. To verify the method, experimental results for N_2–water and N_2–methanol systems are obtained; the estimated values of surface tension for these systems are found to be consistent with the literature values within a deviation of 1%. Furthermore, it is found that the bubble attains its equilibrium shape within 1 s after emerging into the liquid for the N_2–Paratherm NF heat-transfer fluid system under all conditions examined in this study. This finding indicates that for practical purposes, instead of determining the dynamic surface tension, the equilibrium/static surface tension is adequate for characterizing the gas–liquid interfacial properties in the system.

Figure 4c shows the variation of surface tension for N_2 in Paratherm NF heat-transfer fluid with pressure and temperature. The surface tension decreases by 25% and 35% at temperatures of 300 and 351 K, respectively, when the pressure increases from 0.1 MPa to 20 MPa. For this system, the surface tension decreases with increasing temperature by approximately 4% for every 10 K. The effect of temperature on surface tension is more significant than that of pressure.

Rise of single bubbles

The rise velocity of single bubbles of known sizes, U_b, is measured at various pressures ranging from 0.1 MPa to 19.4 MPa for three temperatures, 27, 47 and 78°C. The bubble size is represented by the equivalent spherical diameter, d_e. The results are shown in Figure 5 for (a) 27°C and (b) 78°C. As shown in the figure, for a given bubble size, U_b tends to decrease with increasing pressure at both temperatures. To elucidate the effects of pressure and temperature, or more directly, the effects of physical properties of the gas and liquid phases on the variation of U_b with d_e, the following three predictive equations are considered for comparisons.

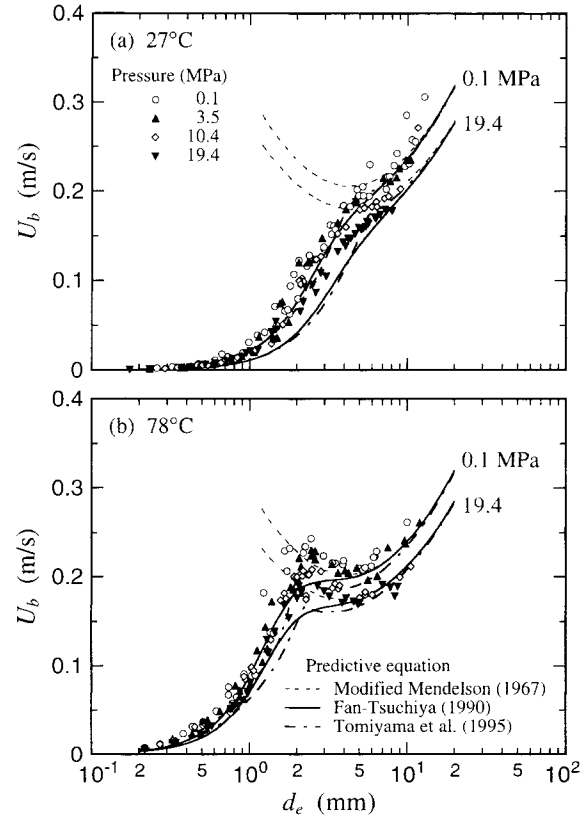

Figure 5. Effect of pressure on terminal rise velocity of single bubbles in Paratherm NF heat-transfer fluid and predicted values at (a) 27°C and (b) 78°C.

1. The Mendelson (1967) equation recently modified by Maneri (1995)

$$U_b = \left[\frac{2c\sigma}{\rho_l d_e} + \left(\frac{\Delta\rho}{\rho_l}\right)\frac{gd_e}{2}\right]^{1/2} \tag{9}$$

is applicable for both single gas bubbles and liquid drops rising/falling in a continuous phase of purified, low-viscosity liquids (immiscible with the drop liquid).

2. The Fan–Tsuchiya (1990) correlation, generalized for high-pressure systems, has a dimensionless form:

$$U_b' = U_b\left(\frac{\rho_l}{\sigma g}\right)^{1/4} = \left\{\left[\frac{Mo^{-1/4}}{K_b}\left(\frac{\Delta\rho}{\rho_l}\right)^{5/4} d_e'^2\right]^{-n} + \left[\frac{2c}{d_e'} + \left(\frac{\Delta\rho}{\rho_l}\right)\frac{d_e'}{2}\right]^{-n/2}\right\}^{-1/n}, \tag{10}$$

where the dimensionless bubble diameter is given by

$$d_e' = d_e(\rho_l g/\sigma)^{1/2}. \tag{11}$$

Three empirical parameters, n, c, and K_b, in Eq. 10 reflect three specific factors governing the rate of bubble rise. They are the contamination level of the liquid phase, variation due to dynamic effects of the surface tension with mono- or multicomponent liquids, and the viscous nature of the surrounding medium. The suggested values of these parameters are:

$$n = \begin{cases} 0.8 & \text{for contaminated liquids} \\ 1.6 & \text{for purified liquids} \end{cases}$$

$$c = \begin{cases} 1.2 & \text{for monocomponent liquids} \\ 1.4 & \text{for multicomponent liquids} \end{cases}$$

$$K_b = \max(K_{b0} Mo^{-0.038}, 12), \tag{12}$$

where

$$K_{b0} = \begin{cases} 14.7 & \text{for aqueous solutions} \\ 10.2 & \text{for organic solvents/mixtures.} \end{cases}$$

3. The Tomiyama et al. (1995) correlation, which is given in terms of drag coefficient $C_D = 4/3g\Delta\rho d_e/(\rho_l U_b^2)$, consists of three equations, depending on the system purity:

$$C_D = \max\left\{\min\left[\frac{16}{Re}(1+0.15Re^{0.687}), \frac{48}{Re}\right], \frac{8}{3}\frac{Eo}{Eo+4}\right\}, \tag{13a}$$

for purified systems;

$$C_D = \max\left\{\min\left[\frac{24}{Re}(1+0.15Re^{0.687}), \frac{72}{Re}\right], \frac{8}{3}\frac{Eo}{Eo+4}\right\}, \tag{13b}$$

for partially contaminated systems; and

$$C_D = \max\left[\frac{24}{Re}(1+0.15Re^{0.687}), \frac{8}{3}\frac{Eo}{Eo+4}\right], \tag{13c}$$

for sufficiently contaminated systems.

In the preceding equations —Eqs. 9, 10, and 13—the dimensionless groups are defined as $Mo = g\Delta\rho\mu_l^4/(\rho_l^2\sigma^3)$, $Re = d_e U_b \rho_l/\mu_l$, and $Eo = g\Delta\rho d_e^2/\sigma$, where $\Delta\rho = \rho_l - \rho_g$. It is noted that U_b can be obtained explicitly from Eq. 9 or 10 for a given d_e as well as gas and liquid physical properties, while it can only be obtained implicitly from Eq. 13.

Figure 5 shows the predictions based on Eqs. 9, 10 and 13. For predictions, measured values of physical properties under various operating pressures and temperatures (see Figure 4) are used. Since the Mendelson equation (Eq. 9) is valid only under inviscid conditions, the limited agreement between the measured and calculated results at the low temperature (Figure 5a) suggests that viscous forces predominate in the bubble rise process. On the other hand, at the high temperature (Figure 5b), there is a strong agreement over the bubble-size range $d_e > 2$ mm, including the sharp breakpoint/peak. This indicates that at high temperature the liquid used in this study tends to behave as a pure inviscid liquid. Note that over the pressure range from 0.1 MPa to 19.4

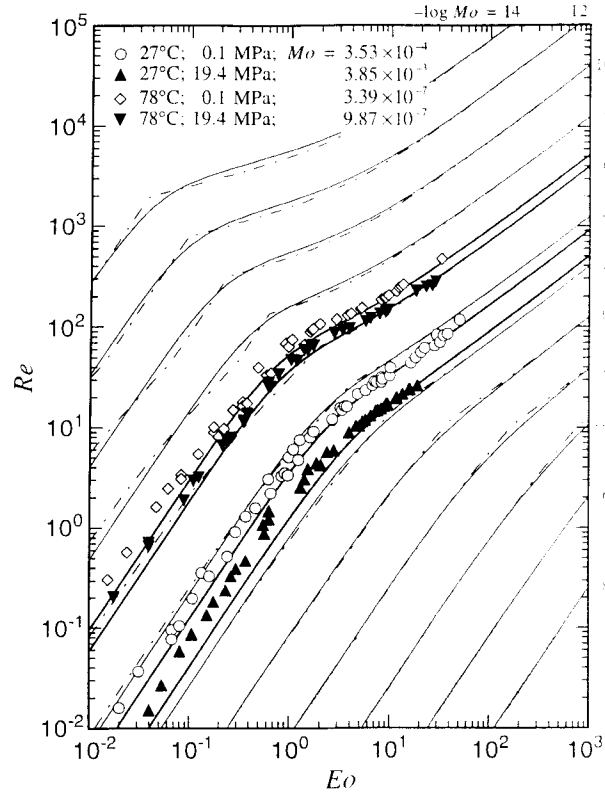

Figure 6. Measured vs. calculated *Re* of single bubbles in Paratherm NF heat-transfer fluid under varied pressure and temperature conditions.

The —— Fan–Tsuchiya (1990) and ——— Tomiyama et al. (1995) relations are plotted at regular intervals of *Mo* values. The —— Fan–Tsuchiya (1990) correlation at measured *Mo* values for comparison with measured *Re-Eo* data.

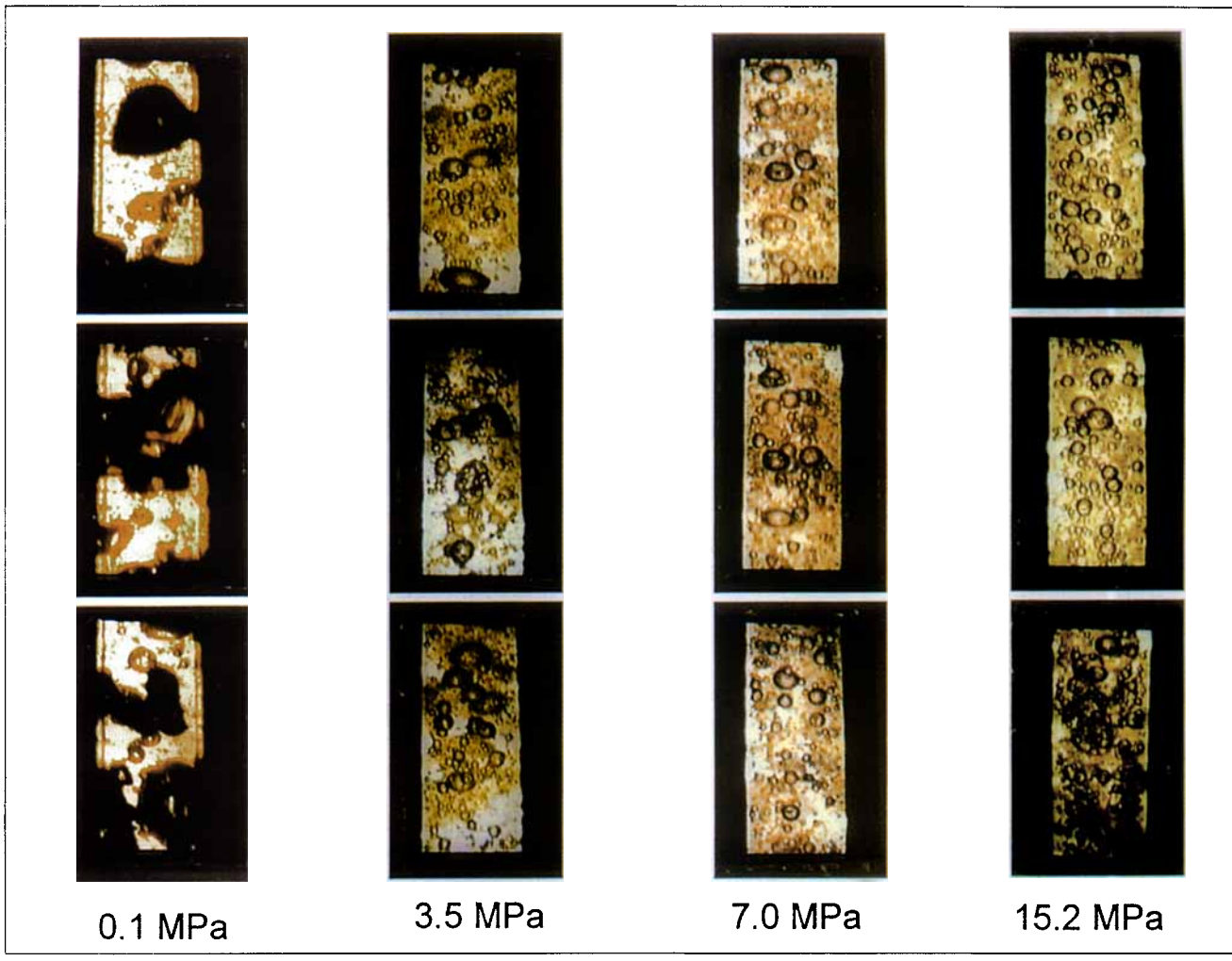

Figure 7. Bubbles under various pressures at $T = 27°C$ and $U_g = 8$ cm/s.

MPa, the liquid viscosity varies from 29 mPa·s to 48 mPa·s at 27°C, whereas it is almost constant within a range from 4.7 mPa·s to 5.2 mPa·s at 78°C.

The Fan–Tsuchiya (1990) correlation (Eq. 10) applied for the present liquid, a pure ($n = 1.6$), multicomponent ($c = 1.4$) organic solvent ($K_{b0} = 10.2$), demonstrates good overall predictive capability except for the high-temperature case, which exhibits a sharp peak near $d_e = 2$ mm (see Figure 5b). The Tomiyama et al. (1995) equation (Eq. 13a) also has good general applicability and predicts the high temperature $d_e = 2$ mm peak; however, it tends to underestimate the U_b values over the rest of the d_e range.

The consistent difference in U_b prevailing between 0.1 and 19.4 MPa for $d_e > 2$ mm is due to the significant increase in gas density (as large as 200-fold increase with pressure from 0.1 MPa to 19.4 MPa). The density effect is accounted for in Eqs. 9 and 10 in terms of $\Delta\rho/\rho_l$ or in Eq. 13 in terms of both $\Delta\rho/\rho_l$ and Eo. As can be seen from the equations and figure, the density difference between the continuous liquid phase and the dispersed gas phase plays an important role in determining U_b, especially for large bubbles.

Figure 6 shows the Re–Eo relationship often utilized in representing the general rise characteristics of single bubbles in liquids (Clift et al., 1978; Bhaga and Weber, 1981). The thin background lines signify the general, quantitative trend for the rise velocity of single bubbles in purified Newtonian liquids under ambient conditions, plotted with constant intervals of log Mo. The figure shows the general agreement in prediction between the Fan–Tsuchiya (1990) correlation (Eq. 10; solid lines) and the Tomiyama et al. (1995) equation (Eq. 13a; dot-dash lines). The present results are plotted in the figure under four conditions, along with the corresponding prediction based on Eq. 10 given by the thick solid lines. By employing accurate values for physical properties of the liquid phase and the gas density at given pressures and temperatures for Eq. 10, the experimental results can be successfully represented over the entire Eo range (i.e., bubble size range) by Eq. 10 as shown in Figure 6.

Dynamics of interactive bubbles: size distribution and underlying mechanisms

In a bubble column, bubbles undergo interactions; they can be weak as in hindered rising or strong as in coalescence and breakup. Under the hindered rising condition, the inherent rise characteristics of single bubbles play an essential role, and the initial/detached bubble size during bubble formation as well as the number density of dispersed bubbles deter-

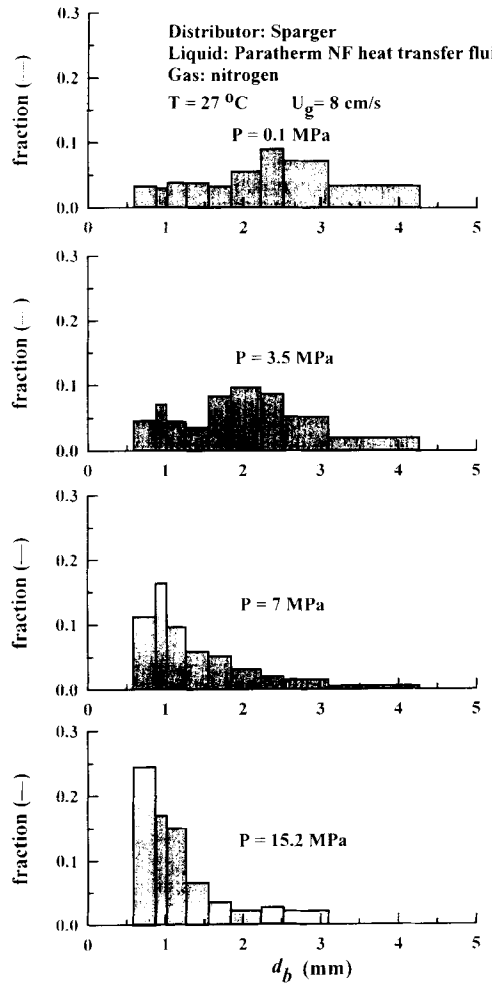

Figure 8. Bubble-size distributions under various pressures at $T = 27°C$ and $U_g = 8$ cm/s.

mines the rise velocity and residence time of the bubbles in the column. For highly interactive bubbles, the dominant factor controlling their dispersion state is their dynamic size variation due to local bubble coalescence and breakup. The bubble-size distribution is evaluated in this study through direct video-enhanced visualization of bubbles at a location 0.40 m above the gas distributor for various pressures under three different temperature and superficial gas velocity conditions: 27°C and 8 cm/s; 27°C and 2 cm/s; and 78°C and 5 cm/s.

Figure 7 shows photographs of bubbles at 27°C and $U_g = 8$ cm/s. Under this condition, as pressure increases from 0.1 to 15.2 MPa, large bubbles gradually disappear. The corresponding distributions of bubble size, d_b, from 0.6 mm to 4.3 mm, are shown in Figure 8. The shift in bubble-size distribution demonstrates the effect of pressure on bubble size. (Although bubbles of d_b less than 0.5 mm existed in the column, the difficulty in quantifying them precluded their inclusion in this study.) It can be seen from the figure that for pressures between 0.1 and 3.5 MPa, the bubble size is widely distributed, with the fraction of bubbles of size larger than 2.5 mm decreasing noticeably with increasing pressure. For pressures greater than 7.0 MPa, the size distribution is appreciably narrower. As the pressure increases from 0.1 to 15.2 MPa, the dominant bubble size shifts from 2.5 to 0.6 mm, and the fraction of bubble sizes between 2 and 4 mm decreases by three-quarters.

Figures 9 and 10 show, respectively, photographs of bubbles and the associated bubble-size distributions for different pressures at 27°C and $U_g = 2$ cm/s. Comparisons of the corresponding photographs in Figures 7 and 9 indicate a general trend that large bubbles disappear progressively with increasing pressure under both conditions. Comparing Figures 8 and 10 shows that the fraction of large bubbles is less at 2 cm/s relative to the fraction of large bubbles at 8 cm/s, especially under lower pressures.

Figures 11 and 12 show, respectively, photographs of bubbles and the corresponding bubble-size distributions at 78°C and $U_g = 5$ cm/s. As can be seen from these figures, although the most prevalent bubble size (0.5–0.6 mm) is the same for all pressures, the fraction of bubbles of a size larger than 2 mm is reduced significantly as the pressure increases from 0.1 MPa to 3.5 Mpa. A comparison between Figures 8 and 12 clearly shows that, at a pressure of 3.5 MPa, the dominant bubble size is reduced from 2 mm at 27°C to 0.5 mm at 78°C.

To illustrate the pressure and temperature effects on the bubble-size distribution, it is necessary to examine the mechanisms of dynamic processes that are responsible for the bubble-size variation, that is, bubble formation, coalescence, and breakup.

Bubble Formation. The mechanism of bubble formation from a single nozzle has been extensively studied under atmospheric pressure (Fan, 1989). At a very low gas velocity, the surface tension and buoyancy forces predominate in the bubble-formation process and the initial bubble size can be estimated from (Davidson and Schuler, 1960)

$$d_b = \left[\frac{6 d_o \sigma}{g(\rho_l - \rho_g)}\right]^{1/3} \tag{14}$$

for single-hole/nozzle gas injectors or multihole gas spargers with adequate hole pitch such as the present ring sparger.

A normalized initial bubble size was obtained by dividing d_b (initial bubble size) at a given pressure by d_{bo} at ambient pressure. This ratio decreases gradually with increasing pressure up to 4–6 MPa, as shown in Figure 13. The simplified force balance as expressed in Eq. 14 is sufficient to support the trend exhibited by the present data on bubble-size distribution at low gas velocity shown in Figure 10. Referring again to Figure 13, further increase in pressure above 6 MPa increases the initial bubble size due to an appreciable reduction in the density difference $\rho_l - \rho_g$. This calculated trend signifies the limitation of Eq. 14, which could not be extended to pressures beyond 4 MPa. As reported in the literature (e.g., LaNauze and Harris, 1974; Idogawa et al., 1987a), increased pressure always leads to a decrease in initial bubble size, even at low gas velocities.

Under high-pressure conditions, other forces need to be taken into account in describing the bubble-formation process. A general force balance, like Pinczewski's (1981) equation, includes the contributions from the pressure difference between the inside and outside of the bubble, inertial force, surface tension force, viscous resistance, and gas momentum:

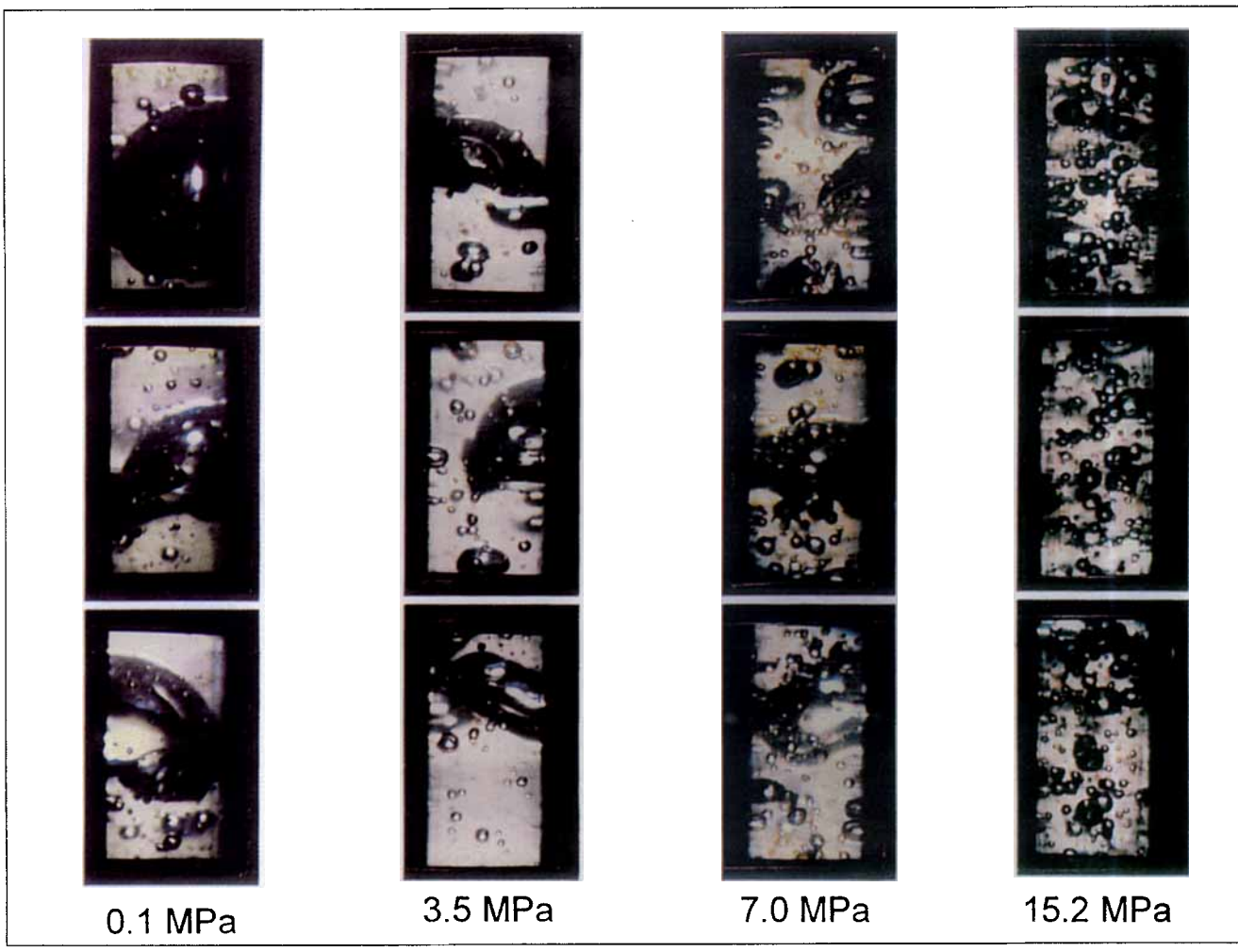

Figure 9. Bubbles under various pressures at $T = 27°C$ and $U_g = 2$ cm/s.

$$P_b - P_h = \rho_l \left[R\frac{d^2R}{dt^2} + \frac{3}{2}\left(\frac{dR}{dt}\right)^2 \right] + \frac{2\sigma}{R} + \frac{4\mu_l}{R}\frac{dR}{dt} - \frac{1}{2}\rho_g u_o^2 \cos^2\theta. \quad (15)$$

Terasaka and Tsuge (1992) demonstrated, in their numerical simulation of the literature results at elevated pressures (Kling, 1962; LaNauze and Harris, 1974; Idogawa et al., 1987a), the importance of the gas-momentum contribution in comparison to the surface-tension contribution. Under such conditions, bubble detachment occurs earlier, resulting in a decrease in the initial bubble size.

Bubble Coalescence. Coalescence of two bubbles occurs in three steps (Chaudhari and Hoffmann, 1994). First, bubbles collide, trapping a small amount of liquid between them. Next, this liquid drains until the liquid film separating the bubbles reaches a critical thickness. Finally, at this critical point, the film ruptures, resulting in bubble coalescence.

Bubble collision can occur by a variety of mechanisms, for example, fluctuations of the turbulent velocity and wake capturing. An increase in viscosity can both damp out the velocity fluctuations and reduce the extent of wake capturing (Crabtree and Bridgwater, 1971). These viscosity effects are more pronounced at elevated pressures because at higher pressures smaller bubbles of uniform size are formed and there is an absence of large bubbles (see Figures 8, 10, and 12). From Figure 4b, viscosity was noted to increase with pressure. Increasing the system pressure thus results in a decrease in the bubble collision rate due to an increase in liquid viscosity.

The duration of film thinning is usually much longer than film rupture (Sagert and Quinn, 1977). Twin injected bubbles form a flat disk of film vertically separating them. Sagert and Quinn found that the rate of thinning of this liquid disk, v_p, can be expressed as

$$v_p = -\frac{dh}{dt} = \frac{8h^3}{3\phi\mu_l R_d^2}\left(\frac{4\sigma}{d_b} + \frac{A_h}{6\pi h^3}\right), \quad (16)$$

where h is the film thickness, R_d is the radius of the disk, and ϕ is a parameter related to surface excess, which is a function of pressure. The term $4\sigma/d_b$ represents the pressure due to curvature of the bubble surface, and the term $A_h/(6\pi h^3)$ represents the pressure due to London forces. The

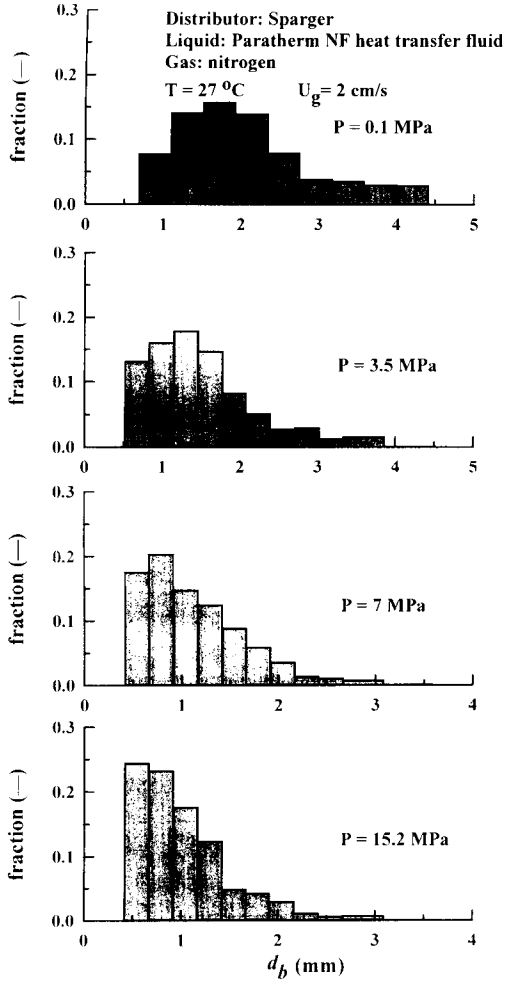

Figure 10. Bubble-size distributions under various pressures at $T = 27°C$ and $U_g = 2$ cm/s.

$4\sigma/d_b$ term is orders of magnitude larger than the $A_h/(6\pi h^3)$ term, which can be neglected. Furthermore, based on Sagert and Quinn's result that ϕ is rather insensitive to pressure, v_p can be shown in simplified form as

$$v_p \propto \frac{8h^3}{3\mu_l R_d^2}\left(\frac{4\sigma}{d_b}\right). \tag{17}$$

Figure 14 shows the decrease of normalized film thinning rate with increasing pressure at three different temperatures. This slowed film thinning can be explained in terms of Eq. 17 by the concomitant reduction in surface tension and the increase in liquid viscosity. Increased temperature results in a rise of the normalized film thinning rate. An analysis of Eq. 17, with full knowledge of the finding from Figure 4b of the tenfold decrease in viscosity over the increasing temperature range, suggests that the rise in v_p is due mainly to the viscosity μ_l.

Bubble Breakup. Two prevalent mechanisms are examined for the pressure effect on bubble breakup. One is based on the Rayleigh–Taylor instability (Taylor, 1950) and the other arises from velocity fluctuations induced by turbulent eddies.

The Rayleigh–Taylor instability occurs in the absence of tangential flow along the gas–liquid interface when gravitational forces acting on the bubble roof predominate over surface tension forces. Bellman and Pennington (1954) suggested that a bubble with a diameter greater than a critical wavelength, λ_c, will form an indentation at the roof and eventually break up. The critical wavelength, or maximum stable bubble size ($d_{b,\max}$) can be calculated from

$$\lambda_c = d_{b,\max} = 2\pi\sqrt{\frac{\sigma}{g(\rho_l - \rho_g)}}. \tag{18}$$

The maximum stable bubble size is thus a primary parameter characterizing the bubble breakup process. In this study, its value is determined from visual observation for each condition. The results are shown in Figure 15 for selected conditions. As can be seen in the figure, the maximum stable bubble size is reduced with increasing pressure for both low and high temperatures, and is smaller at high temperature than that at low temperature for any given pressure. These conditions correspond to the rightmost bands of the bubble-size distribution bar graphs shown in Figures 8, 10 and 12.

Figure 16 shows a comparison between the theoretical prediction of $d_{b,\max}$ obtained using Eq. 18 with the measured *in-situ* physical properties and the present experimental data obtained for various pressures at 78°C. The theoretical prediction shows no significant variation with pressure; however, the experimental data show a dramatic reduction in maximum stable bubble size with increasing pressure up to 4 MPa. This implies that the pressure effect on bubble breakup is not imparted via the Rayleigh–Taylor instability.

To improve the theoretical prediction, Wilkinson (1991) incorporated into Eq. 18 the Kelvin–Helmholtz theory, which accounts for the relative motion between the two phases. Wilkinson proposed that the maximum stable bubble size can be estimated from

$$d_{b,\max} = 2\pi\sqrt{\frac{\sigma}{g(\rho_l - \rho_g)}}\Bigg/\left[\frac{\rho_l}{\rho_l + \rho_g}\frac{\rho_g U_r^2/2}{\sqrt{\sigma g(\rho_l - \rho_g)}} + \sqrt{1 + \frac{\left(\rho_l \rho_g U_r^2/2\right)^2}{(\rho_l + \rho_g)^2 \sigma g(\rho_l - \rho_g)}}\right], \tag{19}$$

where U_r is the relative velocity between the gas and liquid phases at the gas–liquid interface. This relative velocity could reach as high as 1.5 times the terminal bubble rise velocity U_t (Bhaga and Weber, 1981). As shown earlier in Figure 5b, the bubble rise velocity varies weakly with bubble size between 3 and 10 mm under the given conditions and is approximately 0.2 m/s. Thus, assigning a relative velocity of 1.5 times the bubble rise velocity or 0.3 m/s and substituting the measured physical properties into Eq. 19 yields the second theoretical curve, based on the Kelvin–Helmholtz theory, shown in Figure 16. Although the analysis based on this theory gives bet-

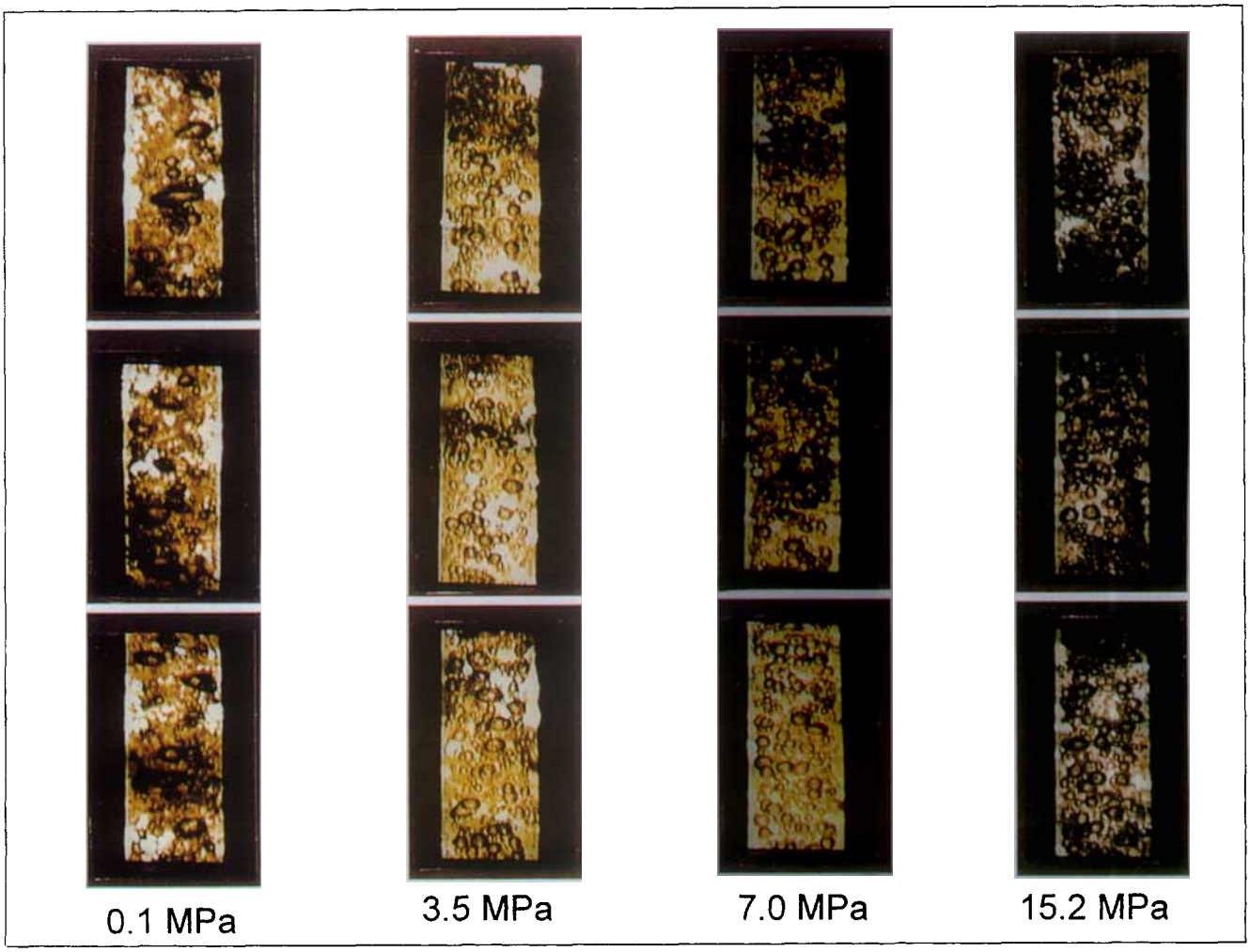

Figure 11. Bubbles under various pressures at $T=78°C$ and $U_g=5$ cm/s.

ter results than the original Rayleigh–Taylor instability theory, both analyses do not properly describe the pressure effect on bubble breakup.

The presence of external disturbances can be taken into account in a mechanism that assumes the velocity fluctuations generated by turbulent eddies to be the primary cause of bubble breakup (e.g., Hinze, 1955). In order for bubble breakup to occur, the energy provided by these disturbances must be sufficient to provide the increase in surface energy required for breakup. This increase in energy appears as surface waves on the bubble upper surface. Surface tension forces tend to stabilize the interface, and viscous forces to slow the growth rate, of unstable surface waves. The critical Weber number defined below accounts for the interacting behavior between the surface tension force and hydrodynamic force:

$$We_c = \frac{\tau}{\sigma/d_{d,\max}}, \tag{20}$$

where $\tau = \rho_l \overline{u^2}$. The rms fluctuating velocity, $\sqrt{\overline{u^2}}$, can be expressed by $p^{1/3}(d_{b,\max}/\rho_l)^{1/3}$ (Hinze, 1955).

Walter and Blanch (1986) used this concept of bubble breakage and proposed the following semiempirical correlation to evaluate the maximum stable bubble size:

$$d_{b,\max} = 1.12 \frac{\sigma^{0.6}}{\rho_l^{0.2} p^{0.4}} \left(\frac{\mu_l}{\mu_g}\right)^{0.1}, \tag{21}$$

where the specific power input is given by $p = \rho_l g U_g$ for bubble columns. As shown in Figure 16, the estimation of $d_{b,\max}$ from Eq. 21 is lower than the experimental data, especially at ambient pressure. Levich (1962) also proposed an equation similar to Eq. 21 by incorporating the ratio of fluid densities:

$$We_c = \frac{\tau}{\sigma/d_{b,\max}} \left(\frac{\rho_g}{\rho_l}\right)^{1/3}. \tag{22}$$

However, in Levich's analysis, the effect of liquid viscosity was not taken into account. Based on Walter and Blanch's analysis, the maximum stable bubble size is proportional to $(\mu_l/\mu_g)^{0.1}$. Incorporation of this viscosity term into Eq. 22 yields the maximum stable bubble size:

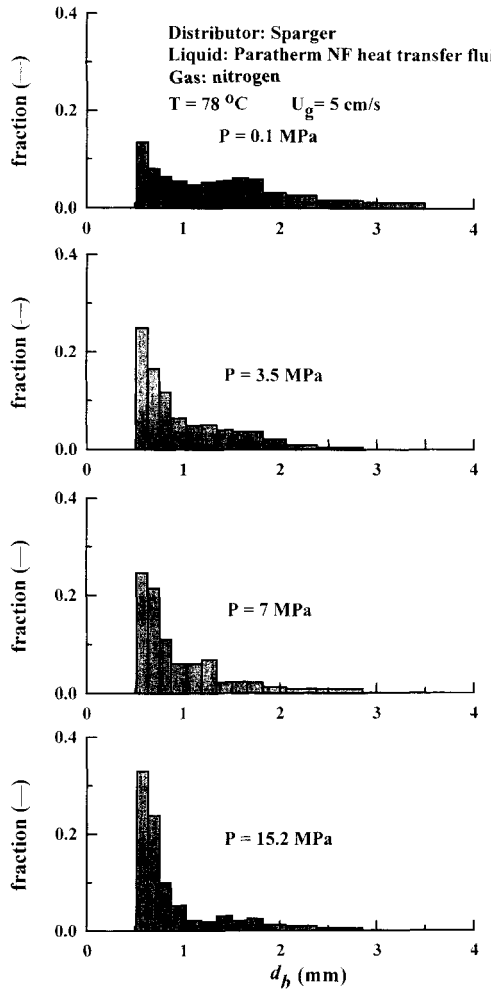

Figure 12. Bubble-size distributions under various pressures at $T = 78°C$ and $U_g = 5$ cm/s.

$$d_{b,\max} = We_c^{0.6} \frac{\sigma^{0.6}}{\rho_g^{0.2} p^{0.4}} \left(\frac{\mu_l}{\mu_g} \right)^{0.1} . \qquad (23)$$

The We_c generally depends on the operating conditions and physical properties. In this study, it is found that the We_c is approximately 0.70 for 78°C and 1.36 for 27°C. Note that these values are within the range reported in the literature (e.g., Sevik and Park, 1973). It is seen from Figure 16 that the modified Levich equation (Eq. 23) gives a trend closest to the experimental data, among all the theoretical models examined in this study.

Based on the model given by Eq. 23 as well as the present experimental data, it can be stated that at a high temperature, the maximum stable bubble size decreases with increasing pressure due to a decrease in surface tension and an increase in gas density. At a low temperature, an appreciable increase in viscosity with pressure would dampen out the fluctuations of liquid velocities, which in turn retards the decreasing rate of maximum stable bubble size caused by a decrease in surface tension and an increase in gas density.

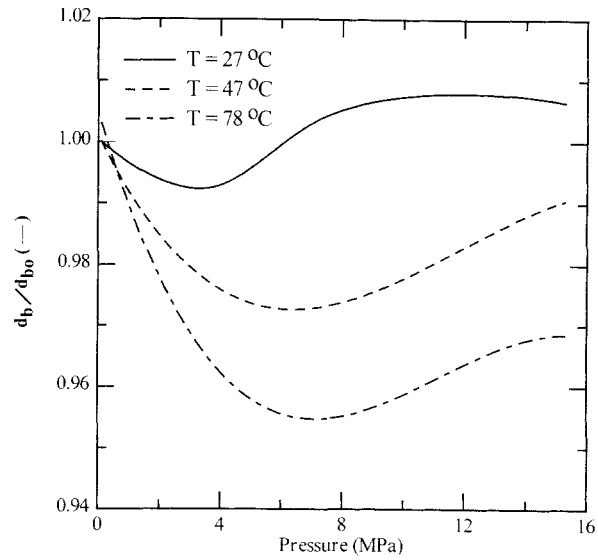

Figure 13. Calculated variation of normalized initial bubble size with pressure based on Eq. 14, for three different temperatures.

Pressure and temperature effects on gas holdup

The gas holdup, ϵ_g, is measured at various pressures ranging from 0.1 MPa to 15.2 MPa for 27, 47 and 78°C. The results are shown in Figure 17 for these three temperatures.

Pressure Effect. As can be seen in Figure 17, for a given temperature and gas velocity, the gas holdup increases with pressure. The result can be interpreted in terms of the variations in bubble-size and rise-velocity distributions. As indicated earlier, with increasing pressure, the bubble-size distribution shifts from larger- to smaller-size bubbles, and the bubble-size distribution becomes narrower (see Figures 8, 10 and 12). For isolated bubbles, the bubble rise velocity de-

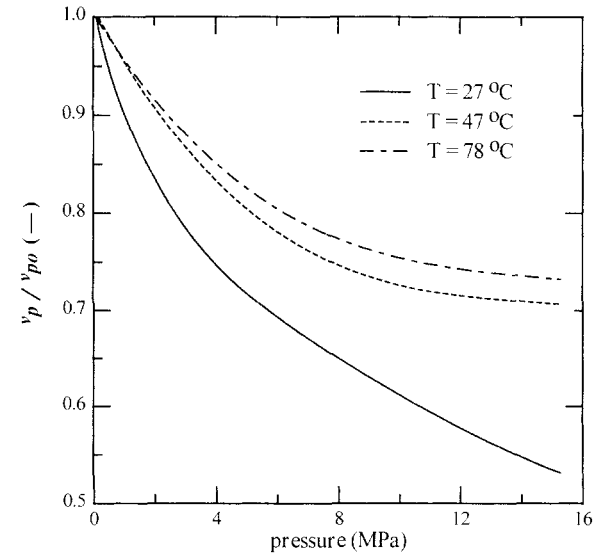

Figure 14. Variation of normalized film-thinning rate with pressure for three different temperatures.

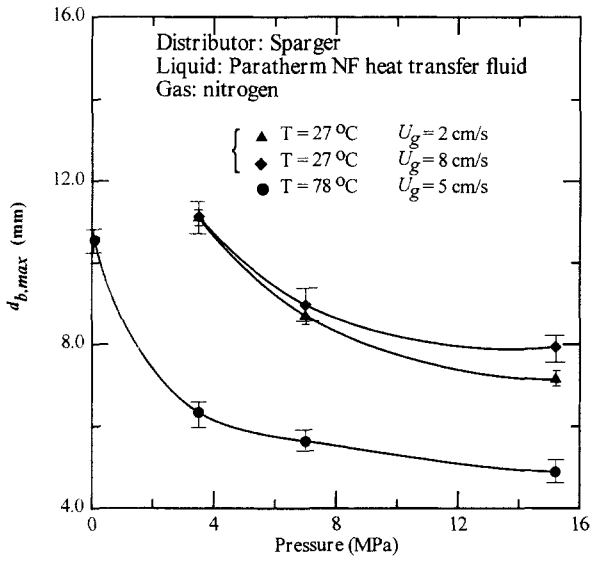

Figure 15. Variation of maximum stable bubble diameter with pressure at 27°C with varying gas flow rates, and 78°C.

creases with increased pressure, especially for bubbles of $d_e > 2$ mm (see Figure 5). A combination of smaller bubble size, narrower size distribution, and reduced rise velocity, contributes to the observed higher gas holdups in an increased pressure system. A more mechanistic reasoning, however, arises from the effect of pressure on density, viscosity, and surface tension, leading to a reduction in initial bubble size and maximum stable bubble size, and the suppression in bubble coalescence rate. Similar observations were made by other researchers (Idogawa et al., 1986; Wilkinson, 1991; Jiang et al., 1995).

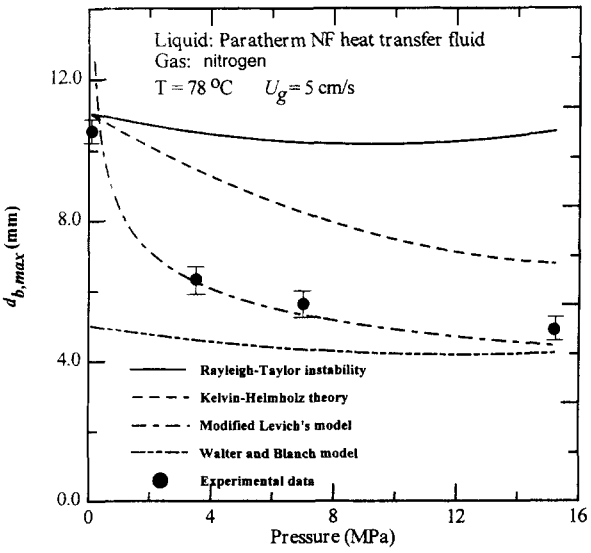

Figure 16. Comparison of predicted maximum stable bubble diameter based on Rayleigh-Taylor instability, Kelvin-Helmholtz theory, modified Levich model, and Walter and Blanch model, with experimental data for 78°C.

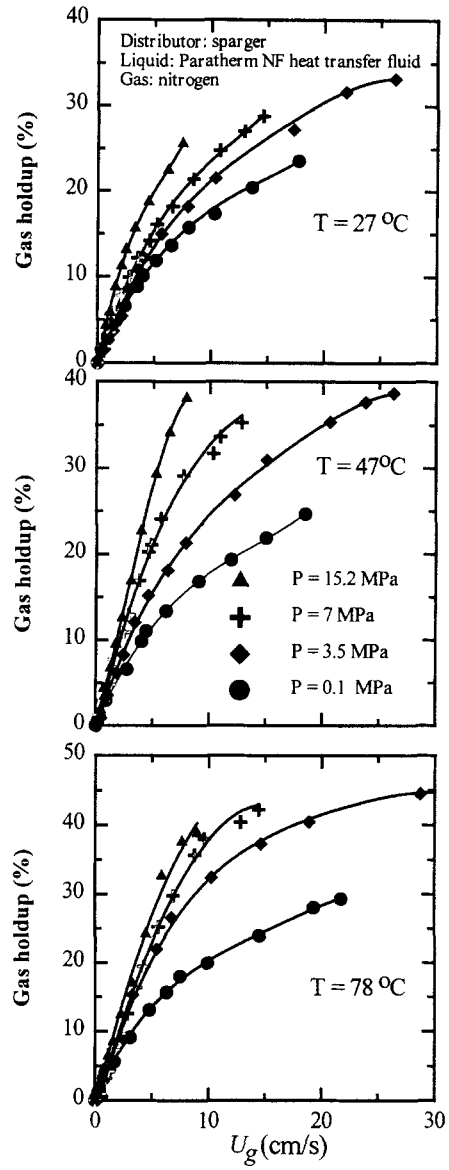

Figure 17. Relationship between gas holdup and gas velocity at various pressures and temperatures.

The pressure effect is most pronounced at higher gas velocities for all temperatures, as shown in Figure 17. This behavior is given in Figure 18, which shows the variation of gas holdup with pressure at two different gas velocities, $U_g = 2$ and 8 cm/s. The figure indicates that the rate of increase in gas holdup with pressure at 8 cm/s is greater than that at 2 cm/s. The most important factor contributing to this difference lies in local bubble dynamics, which are reflected in the observed bubble-size distribution (Figure 8 vs. Figure 10). The maximum stable bubble size, however, is almost the same for $U_g = 2$ and 8 cm/s (see Figure 15).

The response of the gas holdup to the pressure variation depends on temperature. From Figure 17, it can be seen that while at 27°C the holdup gradually increases between any two isobars, at 78°C the holdup difference between two isobars becomes much less for a higher pressure compared to that

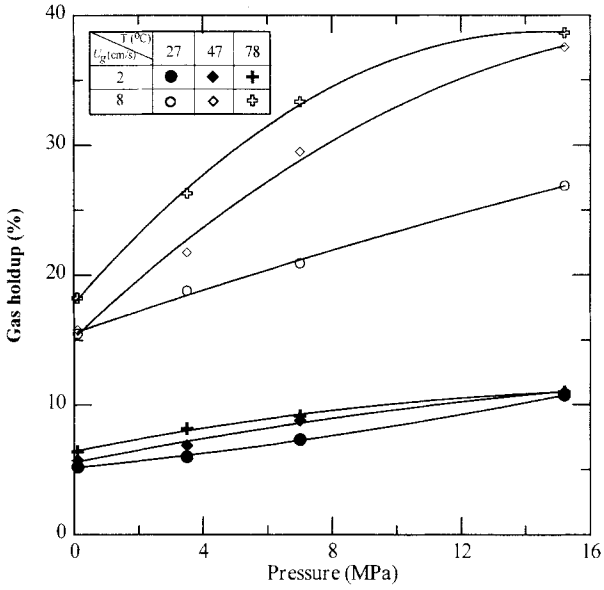

Figure 18. Pressure effect on gas holdup in two gas velocities $U_g = 2$ and 8 cm/s.

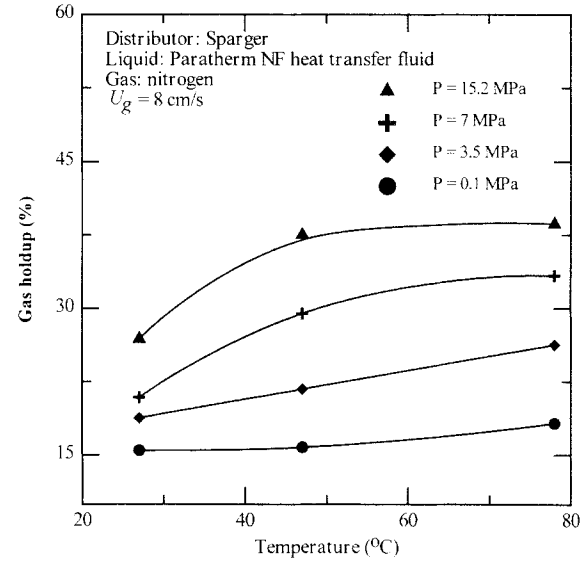

Figure 19. Temperature effect on gas holdup for various pressures at $U_g = 8$ cm/s.

between ambient pressure and 3.5 MPa. The maximum stable bubble size shown in Figure 15 exhibits a similar trend; at 27°C, the change in the rate of $d_{b,\max}$ reduction with increasing pressure occurs gradually over the given pressure range, while at 78°C, the change is sharp at pressures below 4 MPa and progressive above 4 MPa.

At a low temperature, the increase in liquid viscosity associated with an increase in pressure is substantial, which accounts for the increase in the maximum stable bubble size. On the other hand, the surface tension decreases with increasing pressure, which decreases bubble stability. Besides these counteracting effects, the increase in gas momentum due to an increase in pressure tends to decrease the initial bubble size. Both the increase in gas momentum and decrease in surface tension promote a higher gas holdup, while the increase in liquid viscosity decreases the gas holdup. This explains the smaller gas holdup differences at the lower temperature. The larger difference in gas holdup at 78°C arises from a negligible influence of the liquid viscosity at this temperature (see Figure 4b).

Temperature Effect. For a fixed pressure and gas velocity, the temperature effect on gas holdup is complex, but an increase in temperature generally increases the gas holdup, as shown in Figure 17. This general trend is due to the dominant role of associated reduction in liquid viscosity and surface tension, which leads to a smaller average bubble size and a narrower bubble-size distribution; the associated increase in gas density often plays a secondary role. The same argument can be used to illustrate the contradicting results between Grover et al.'s (1986) and Zou et al.'s (1988) noted earlier. In Grover et al.'s air–water system, temperature did not significantly influence the viscosity and surface tension of water. The effect of increasing temperature on decreasing gas density was more dominant, which increased the bubble size; hence, the gas holdup decreased with increasing temperature in Grover et al.'s case. Zou et al.'s case followed the general trend shown earlier.

The effect of temperature on gas holdup for various pressures at a gas velocity of 8 cm/s is shown in Figure 19. It can be seen that the concavity of the isobars changes from upward to downward as the pressure increases from 0.1 to 15.2 MPa. Based on the trend in these curves, a further increase in pressure would result in the differences between the isobars becoming narrower over the same temperature range. This is a result of the continual decrease in surface tension with increasing temperature, while the liquid viscosity is no longer affected to any significant degree by temperature at higher temperatures for all pressures. Note that for ambient pressure, the gas holdup only increases by 2% when the temperature is increased from 27 to 78°C; for 15.2 MPa, however, the gas holdup increases by 12%.

Concluding Remarks

Variations of *in-situ* physical properties including viscosity, surface tension, and gas density with pressure and temperature need to be taken into consideration when accounting for hydrodynamics and transport behavior of the bubble column. For single bubbles, the bubble rise velocity exhibits distinct dependency on both pressure and temperature; the bubble rise velocity can only be reasonably predicted by the existing equations when the dependency of the physical properties of the gas and liquid phases on pressure and temperature are accounted for. Local interactive bubble dynamics, which are reflected in the observed bubble-size distribution in the column, can be interpreted on the basis of bubble formation, coalescence, and breakup mechanisms for high-pressure conditions. In particular, the bubble breakup mechanism for predicting proper dependence of the maximum stable bubble size on pressure and temperature is found to be associated with the external disturbances on bubbles induced by turbulent eddies. At a high temperature, the maximum stable bubble size decreases with increasing pressure due to a decrease in surface tension and an increase in gas density; at a low temperature, a substantial increase in viscosity with increasing

pressure reduces the fluctuations of liquid velocities, and thus retards the decrease in the maximum stable bubble size.

Elevating pressure and/or temperature increases gas holdup, but the increasing rate depends on the operating conditions and the dependency of fluid physical properties on pressure and temperature. A smaller increasing rate in gas holdup upon increasing pressure at a lower temperature arises from the fact that both an increase in gas momentum and a decrease in surface tension give rise to a higher gas holdup while an increase in liquid viscosity hampers an increase in gas holdup. A larger increasing rate in gas holdup at a higher temperature arises from a negligible effect of the liquid viscosity, which is substantially low and essentially invariant with pressure. At a given pressure, the effect of increasing temperature on gas holdup is complex, but it generally yields a positive contribution. This general trend is due to the dominant role of associated reduction in liquid viscosity and surface tension, which leads to smaller maximum stable and average bubble sizes and a narrower bubble-size distribution. The gas-density effect often plays a secondary role.

Acknowledgments

The work was supported by National Science Foundation Grant CTS-9528380. We are grateful to Mr. G. B. Bass for helpful assistance on the experimental work.

Notation

A_h = Hamaker–London constant, J
d_e = diameter of a sphere having the same volume as the bubble, m
d_o = orifice diameter, m
D = column diameter, m
Eo = Eötvös number $g\Delta\rho d_e^2/\sigma$
g = gravitational acceleration, m/s^2
Mo = Morton number $g\Delta\rho\mu_l^4/(\rho_l^2\sigma^3)$
p = specific power input, W/m^3
P_b = pressure inside a bubble, Pa
P_h = pressure outside a bubble, Pa
Re = bubble Reynolds number $d_e U_b \rho_l/\mu_l$
s = arc length from bubble nose, m
t = time, s
T = temperature, K
T_b = boiling temperature, K
u_o = gas velocity through orifice, m/s
U_g = superficial gas velocity, m/s
v_{po} = liquid-film thinning rate at ambient pressure, m/s
We_c = critical Weber number
x = horizontal coordinate defined in Figure 2, m
z = downward coordinate defined in Figure 2, m
Z = vertical distance above gas distributor, m
$\Delta\rho = \rho_l - \rho_g$, kg/m^3
μ_g = gas viscosity, Pa·s
μ_l = liquid viscosity, Pa·s
ρ_g = gas density, kg/m^3
ρ_l = liquid density, kg/m^3

Literature Cited

Bellman, R., and R. H. Pennington, "Effects of Surface Tension and Viscosity on Taylor Instability," *Q. J. Appl. Math.*, **51**, 151 (1954).
Bhaga, D., and M. E. Weber, "Bubbles in Viscous Liquids: Shapes, Wakes. and Velocities," *J. Fluid Mech.*, **105**, 61 (1981).
Chabot, J., and H. I. de Lasa, "Gas Holdups and Bubble Characteristics in a Bubble Column Operated at High Temperature," *Ind. Eng. Chem. Res.*, **32**, 2595 (1993).
Chaudhari, R. V., and H. Hoffmann, "Coalescence of Gas Bubbles in Liquids," *Rev. Chem. Eng.*, **10**, 131 (1994).
Chiba, S., K. Idogawa, Y. Maekawa, H. Moritomi, N. Kato, and T. Chiba, "Neutron Radiographic Observation of High Pressure Three-Phase Fluidization," *Fluidization VI*, J. R. Grace, L. W. Shemilt, and M. A. Bergougnou, eds., Engineering Foundation, New York, p. 523 (1989).
Clark, K. N., "The Effect of High Pressure and Temperature on Phase Distributions in a Bubble Column," *Chem. Eng. Sci.*, **45**, 2301 (1990).
Clift, R., J. R. Grace, and M. E. Weber, *Bubbles, Drops, and Particles*, Academic Press, New York (1978).
Crabtree, J. R., and J. Bridgwater, "Bubble Coalescence in Viscous Liquids," *Chem. Eng. Sci.*, **26**, 839 (1971).
Davidson, J. F., and B. O. G. Schuler, "Bubble Formation at an Orifice in an Inviscid Liquid," *Trans. Inst. Chem. Eng.*, **38**, 335 (1960).
Deam, J. R., and R. N. Maddox, "Interfacial Tension in Hydrocarbon Systems," *J. Chem. Eng. Data*, **15**, 216 (1970).
de Bruijn, T. J. W., J. D. Chase, and W. H. Dawson, "Gas Holdup in a Two-Phase Vertical Tubular Reactor at High Pressure," *Can. J. Chem. Eng.*, **66**, 330 (1988).
Deckwer, W.-D., *Bubble Column Reactors*, Wiley, New York (1992).
Deckwer, W.-D., Y. Louisi, A. Zaidi, and M. Ralek, "Hydrodynamic Properties of the Fischer-Tropsch Slurry Process," *Ind. Eng. Chem. Process Des. Dev.*, **19**, 699 (1980).
Fan, L.-S., *Gas-Liquid-Solid Fluidization Engineering*, Butterworths, Stoneham, MA (1989).
Fan, L.-S., and K. Tsuchiya, *Bubble Wake Dynamics in Liquids and Liquid-Solid Suspensions*, Butterworth-Heinemann, Stoneham, MA (1990).
Grover, G. S., C. V. Rode, and R. V. Chaudhari, "Effect of Temperature on Flow Regimes and Gas Hold-up in a Bubble Column," *Can. J. Chem. Eng.*, **64**, 501 (1986).
Haam, S., "Multiphase Research on Two-Phase Dispersion Column," PhD Thesis, The Ohio State Univ., Columbus (1996).
Hinze, J. O., "Fundamentals of the Hydrodynamic Mechanism of Splitting in Dispersion Processes," *AIChE J.*, **1**, 289 (1955).
Idogawa, K., K. Ikeda, T. Fukuda, and S. Morooka, "Behavior of Bubbles of the Air-Water System in a Column under High Pressure," *Int. Chem. Eng.*, **26**, 468 (1986).
Idogawa, K., K. Ikeda, and T. Fukuda, "Formation and Flow of Gas Bubbles in a Pressurized Bubble Column with a Single Orifice or Nozzle Gas Distributor," *Chem. Eng. Commun.*, **59**, 201 (1987a).
Idogawa, K., K. Ikeda, T. Fukuda, and S. Morooka, "Effect of Gas and Liquid Properties on the Behavior of Bubbles in a Column under High Pressure," *Int. Chem. Eng.*, **27**, 93 (1987b).
Jasper, J. J., "The Surface Tension of Pure Liquid Compounds," *J. Phys. Chem. Ref. Data*, **1**, 841 (1972).
Jennings, J. W., Jr., and N. R. Pallas, "An Efficient Method for the Determination of Interfacial Tensions from Drop Profiles," *Langmuir*, **4**, 959 (1988).
Jiang, P., D. Arters, and L.-S. Fan, "Pressure Effects on the Hydrodynamic Behavior of Gas-Liquid-Solid Fluidized Beds," *Ind. Eng. Chem. Res.*, **31**, 2322 (1992).
Jiang, P., T.-J. Lin, X. Luo, and L.-S. Fan, "Flow Visualization of High Pressure (21 MPa) Bubble Column: Bubble Characteristics," *Trans. Inst. Chem. Eng.*, Part A, **73**, 269 (1995).
Kling, G., "Über die Dynamik der Blasenbildung Beim Begasen von Flüssigkeiten Unter Druck," *Int. J. Heat Mass Transfer*, **5**, 211 (1962).
Kuo, J. C. W., "Two-Stage Process for Conversion of Synthesis Gas to High Quality Transportation Fuels," Final Rep. to the U.S. Dept. of Energy for Contract DE-AC22-83PC60019, Mobil Research and Development Co., Paulsboro, NJ (1985).
LaNauze, R. D., and I. J. Harris, "Gas Bubble Formation at Elevated System Pressures," *Trans. Inst. Chem. Eng.*, **52**, 337 (1974).
Levich, V. G., *Physicochemical Hydrodynamics*, Prentice Hall, Englewood Cliffs, NJ (1962).
Lin, T.-J., and L.-S. Fan, "Characteristics of High-Pressure Liquid-Solid Fluidization," *AIChE J.*, **43**, 45 (1997).
Maneri, C. C., "New Look at Wave Analogy for Prediction of Bubble Terminal Velocities," *AIChE J.*, **41**, 481 (1995).
Massoudi, R., and A. D. King, Jr., "Effect of Pressure on Surface Tension of Water. Adsorption of Low Molecular Weight Gases on Water at 25°C," *J. Phys. Chem.*, **78**, 2262 (1974).
Mendelson, H. D., "The Prediction of Bubble Terminal Velocities from Wave Theory," *AIChE J.*, **13**, 250 (1967).

Pinczewski, W. V., "The Formation and Growth of Bubbles at a Submerged Orifice," *Chem. Eng. Sci.*, **36**, 405 (1981).
Reilly, I. G., D. S. Scott, T. J. W. de Bruijn, and D. MacIntyre, "The Role of Gas Phase Momentum in Determining Gas Holdup and Hydrodynamic Flow Regimes in Bubble Column Operations," *Can. J. Chem. Eng.*, **72**, 3 (1994).
Sagert, N. H., and M. J. Quinn, "Influence of High-Pressure Gases on the Stability of Thin Aqueous Films," *J. Colloid Interface Sci.*, **61**, 279 (1977).
Sevik, M., and S. H. Park, "The Splitting of Drops and Bubbles by Turbulent Fluid Flow," *Trans. ASME J. Fluids Eng.*, **95**, 53 (1973).
Slowinski, E. J., Jr., E. E. Gates, and C. E. Waring, "The Effect of Pressure on the Surface Tensions of Liquids," *J. Phys. Chem.*, **61**, 808 (1957).
Stephan, K., and K. Lucas, *Viscosity of Dense Fluids*, Plenum Press, New York (1979).
Taylor, G. I., "The Instability of Liquid Surfaces When Accelerated in a Direction Perpendicular to Their Planes," *Proc. R. Soc. Lond.*, **A201**, 192 (1950).
Terasaka, K., and H. Tsuge, "Bubble Formation at an Orifice in Liquid under Highly Pressurized Conditions," *Int. J. Eng. Fluid Mech.*, **5**, 439 (1992).
Tomiyama, A., I. Kataoka, and T. Sakaguchi, "Drag Coefficients of Bubbles (1st Report, Drag Coefficients of a Single Bubble in a Stagnant Liquid)," *Nippon Kikai Gakkai Ronbunshu B Hen*, **61**(587), 2357 (1995).
Walter, J. F., and H. W. Blanch, "Bubble Break-Up in Gas-Liquid Bioreactors: Break-Up in Turbulent Flows," *Chem. Eng. J.*, **32**, B7 (1986).
Wilkinson, P. M., "Physical Aspects and Scale-Up of High-Pressure Bubble Columns," PhD Thesis, Univ. of Groningen, Groningen, The Netherlands (1991).
Wilkinson, P. M., and L. L. van Dierendonck, "Comments on 'Studies on Gas Holdup in a Bubble Column Operated at Elevated Temperatures,'" *Ind. Eng. Chem. Res.*, **29**, 927 (1990).
Zou, R., X. Jiang, B. Li, Y. Zu, and L. Zhang, "Studies on Gas Holdup in a Bubble Column Operated at Elevated Temperatures," *Ind. Eng. Chem. Res.*, **27**, 1910 (1988).

Manuscript received Aug. 11, 1997, and revision received Jan. 2, 1998.